Pergamon

Acta mater. Vol. 46, No. 16, pp. 5873–5882, 1998

Printed in Great Britain
PII: S1359-6454(98)00234-1
1359-6454/98 $19.00 + 0.00

STRUCTURAL DISORDERING IN AMORPHOUS $Pd_{40}Ni_{40}P_{20}$ INDUCED BY HIGH TEMPERATURE DEFORMATION

P. DE HEY, J. SIETSMA† and A. VAN DEN BEUKEL

Laboratory of Materials Science, Delft University of Technology, Rotterdamseweg 137, 2628 AL Delft, Netherlands

(Received 12 January 1998; accepted 4 June 1998)

Abstract—The influence of plastic deformation on the structural state of amorphous $Pd_{40}Ni_{40}P_{20}$ is investigated by means of tensile test measurements as a function of temperature, strain rate and pre-annealing time. The structural state of the material after the deformation is investigated by means of differential scanning calorimetry (DSC). It is found that amorphous $Pd_{40}Ni_{40}P_{20}$, when pre-annealed into its metastable equilibrium state, shows a large strain softening effect when deformed at temperatures close to the glass transition temperature. The strain softening effect is less pronounced or even absent in samples that are only briefly pre-annealed. The DSC traces show that the structural state of the material disorders during the deformation and that the material reaches a strain rate and temperature dependent equilibrium state, which differs from the thermal equilibrium state. It is shown that the strain softening effect is caused by the creation of additional free volume during the deformation. © *1998 Acta Metallurgica Inc. Published by Elsevier Science Ltd. All rights reserved.*

1. INTRODUCTION

The high temperature viscous properties of metallic glasses, and the influence of thermal annealing on these properties, have been the subject of numerous studies [1–4]. The viscosity of the glass is of particular interest, since it is directly related to the atomic mobility in these metastable systems. By annealing a metallic glass below the crystallization temperature, the quenched-in disorder is reduced, resulting in a lower atomic mobility and consequently profound changes in the viscosity. It was found in the earliest studies that the viscosity of metallic glasses increases linearly with time during high temperature annealing (e.g. Ref. [1]) and that the increase in the viscosity can be as large as four orders of magnitude. The processes that govern the underlying structural changes are usually referred to as structural relaxation. For relatively stable metallic glasses, i.e. glasses with a low critical cooling rate which show the calorimetric glass transition [4, 5] and a wide supercooled liquid region prior to crystallization, the viscosity was found to level off at a plateau value when annealed at temperatures close to the glass transition temperature T_g for long enough times [4]. The plateau value of the viscosity was found to be fully reversible with respect to temperature, indicating that the material can reach a metastable equilibrium state at temperatures close to T_g.

An unfavourable effect of annealing is the embrittlement of the glass, which has been reported for several alloys [6–8]. Recently, Inoue *et al.* [8] found that amorphous $La_{55}Al_{25}Ni_{20}$, embrittled by annealing well below the glass transition temperature, can be reductilized by high strain rate deformation at temperatures above the glass transition temperature. In other words, the material regains its ability to flow during the high temperature deformation. The calorimetric glass transition peak of the material after deformation showed distinct changes with increasing strain rate, which suggests that high temperature deformation itself induces structural changes in the glass, which enhance the ductility.

In the present paper, we will present a systematic investigation of deformation induced structural changes. Such a study provides information about the mechanism of viscous flow in metallic glasses and hence the atomic mobility. The material under investigation here is amorphous $Pd_{40}Ni_{40}P_{20}$, since a number of physical properties of this material, including the viscosity [4] and the calorimetric glass transition [9], and the influence of structural relaxation on these properties, has been thoroughly investigated in the past. This allows both a qualitative and quantitative investigation of the processes occurring during deformation, using the previously established relation between the shape of the calorimetric glass transition peak and the structural state of the material.

†To whom all correspondence should be addressed.

2. THE FREE VOLUME DESCRIPTION OF THE STRUCTURAL STATE OF $Pd_{40}Ni_{40}P_{20}$

In the model proposed by Spaepen [10], homogeneous viscous flow of metallic glasses at high temperatures takes place at so-called flow defects, i.e. sites in the material at which thermally activated local shear events can occur. For tensile conditions, a convenient form of Spaepen's relation is

$$\dot{\varepsilon} = 2c_f k_f \frac{\varepsilon_0 v_0}{\Omega} \sinh\left(\frac{\sigma \varepsilon_0 v_0}{2kT}\right) \tag{1}$$

with $\dot{\varepsilon}$ the strain rate, σ the tensile stress, c_f the concentration of flow defects, k_f a rate factor, ε_0 the local strain, v_0 the volume of the local sheared region, Ω the atomic volume, k Boltzmann's constant and T the temperature. The viscosity $\eta \equiv \sigma/3\dot{\varepsilon}$ is therefore inversely proportional to c_f. Most studies on the viscous flow properties have been done in the low stress regime, where viscous flow is Newtonian, since $\sinh(\sigma\varepsilon_0 v_0/2kT) \approx \sigma\varepsilon_0 v_0/2kT$. The high stress regime of equation (1), however, has not been thoroughly tested. In general, deviations from Newtonian behaviour are found to be small [11].

Duine *et al.* [4] have shown that during isothermal annealing at temperatures close to the glass transition temperature, the viscosity of a-PdNiP reaches a plateau value. Since $\eta \propto c_f^{-1}$, this means that the defect concentration reaches a constant value. The plateau value of the viscosity was found to be fully reversible with respect to the temperature, meaning that the material reaches a metastable equilibrium defect concentration $c_{f,eq}$. It was found in Ref. [4] that the change in the defect concentration towards the equilibrium defect concentration is described by the rate equation

$$\frac{dc_f}{dt} = -k_r c_f (c_f - c_{f,eq}) \tag{2}$$

with $k_r = \nu_r \exp(-Q_r/kT)$ a rate constant with activation energy Q_r and pre-exponential factor ν_r. When $c_f \gg c_{f,eq}$, equation (2) and $\eta \propto c_f^{-1}$ imply a linear increase of η with time. The free volume model [12] relates the defect concentration to the free volume according to

$$c_f = \exp\left(-\frac{1}{x}\right) \tag{3}$$

where $x = \langle v \rangle / \gamma v^*$ is the so-called reduced free volume, with $\langle v \rangle$ the average free volume per atom, v^* the amount of free volume needed for atomic movement to take place and γ an overlap factor between 0.5 and 1. In thermal equilibrium, the free volume x_{eq} has a similar relation to $c_{f,eq}$, and depends linearly on the temperature by

$$x_{eq} = \frac{T - T_0}{B} \tag{4}$$

where B and T_0 are two material constants.

Equations (2)–(4) have been found to not only describe the change in the viscosity of a-PdNiP during isothermal annealing, but also the change in Young's modulus [13] and electrical resistivity [14], using a single set of values for the material parameters B, T_0, ν_r and Q_r. For the latter two properties, which do not directly depend on the atomic mobility, it was assumed that the change in the property is proportional to the change in reduced free volume x rather than to the defect concentration. Moreover, van den Beukel and Sietsma [15] have shown that solving equation (2) under the conditions that occur during a DSC experiment, i.e. at constant heating rate, covers the basic features of the calorimetric glass transition, using the simple assumption that the heat release rate of the amorphous sample dH/dt is proportional to the rate change of the free volume dx/dt. This was later elaborated for a-PdNiP by Tuinstra *et al.* [9]. In particular, by performing an extensive set of DSC experiments on PdNiP samples that had been submitted to different pre-annealing treatments, Tuinstra *et al.* found a monotonous relation between the height of the glass transition peak Δc_p and the amount of free volume x_0, which characterizes the structural state of the sample at the beginning of the DSC scan. In the study of Tuinstra *et al.* the parameter x_0 depends on the thermal history of the sample through the same set of equations (2)–(4). In this paper, we will use the relation between Δc_p and x_0 as established by Tuinstra *et al.* to deduce the free volume of samples that have undergone a heat treatment and deformation.

3. EXPERIMENTAL

Amorphous $Pd_{40}Ni_{40}P_{20}$ was produced by melt spinning in the form of a ribbon with a width of 2.8 mm. Sample ribbons with a gauge length of about 200 mm were cut from the master ribbon and the sample thickness was determined from the mass of the sample, using the density of 9480 kg/m^3 reported in Ref. [16]. The average sample thickness determined in this way is 18 μm with variations within ± 2 μm.

The tensile tests were performed on a tensile testing machine constructed in the laboratory workshop, with a cylindrical furnace placed vertically between a fixed grip and a moveable, constant velocity, grip. The temperature profile in the furnace is within 0.5 K over long periods of time and within 1 K over a length of about 100 mm. The temperature drops off sharply at the ends of the furnace. Therefore, given the strong temperature dependence of the plastic flow [4] and anelastic relaxation [17] of this material, contributions of plastic and anelastic strain outside the hot zone are neglected. In that case, the stress–strain relation in the hot zone of the sample can be derived from the total measured elongation as follows. After a certain time t the

total elongation ΔL of a sample with length L is given by $v_g t$, with v_g the constant velocity of the moving grip. If L^H is the length of the hot zone, the total elongation, being the sum of the elastic, anelastic and plastic elongation in the hot zone of the sample ($\varepsilon_e^H L^H$, $\varepsilon_a^H L^H$ and $\varepsilon_p^H L^H$, respectively) and the elastic elongation $\varepsilon_e^C(L - L^H)$ outside the hot zone, is given by

$$\Delta L = \varepsilon_e^C(L - L^H) + (\varepsilon_e^H + \varepsilon_a^H + \varepsilon_p^H)L^H = v_g t \quad (5)$$

with $L \approx 200$ mm and $L^H \approx 100$ mm. Rearranging equation (5) and substituting $\varepsilon = \varepsilon_e^H + \varepsilon_a^H + \varepsilon_p^H$ leads to

$$\varepsilon = \frac{v_g}{L^H} t - \varepsilon_e^C \frac{L - L^H}{L^H} = \dot{\varepsilon} \cdot t - \frac{\sigma}{E}\frac{L - L^H}{L^H} \quad (6)$$

where $\dot{\varepsilon} = v_g / L^H$ is the strain rate in the hot zone, E is Young's modulus at room temperature (which was measured to be $E = 96$ GPa, in accordance with the value reported by Davis *et al.* [16]) and σ is the stress F/A, with F the force measured by a semiconductor load cell and A the cross-sectional area of the sample. Since the elastic strain outside the hot zone will be small compared to the plastic strain within the hot zone, the second term on the right-hand side of equation (6) will be negligible when the material starts to deform plastically. The actual strain rate $d\varepsilon/dt$ in the hot zone of the sample then equals the constant $\dot{\varepsilon}$. Since L^H remains constant during the tensile test, ε and $\dot{\varepsilon}$ in equation (6) are the true strain and true strain rate, respectively. The true stress $\sigma = F/A$ can be derived from a mass balance over the hot zone of the sample to be given by $\sigma = \sigma_0 \exp(\varepsilon)$, with $\sigma_0 = F/A_0$ and A_0 the initial cross-sectional area of the sample.

The set-up is placed inside a vacuum chamber. A constant flow of helium is applied to optimize the heat transfer during the test and to prevent oxidation of the samples. Pre-annealing of the specimens was carried out *in situ*, immediately followed by tensile testing. The tests were stopped directly after failure of the specimen or after a certain amount of deformation. Failure of a specimen always took place in the hot zone of the specimen.

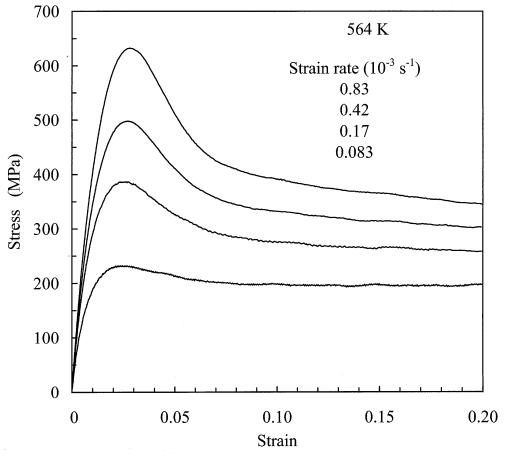

Fig. 1. True stress vs true strain curves for a-PdNiP, pre-annealed for 5000 s at 564 K, measured at 564 K at the indicated strain rates.

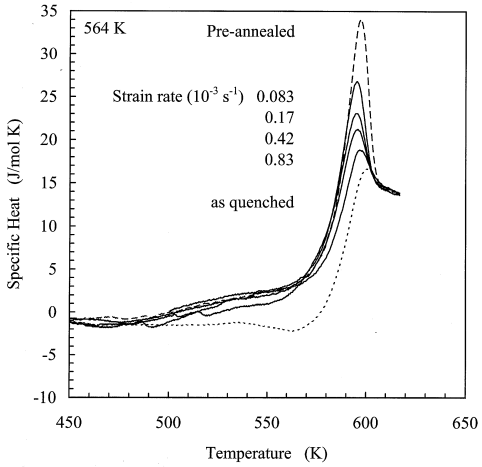

Fig. 2. Solid lines: experimental DSC traces of the samples from Fig. 1 after the deformation. Dashed line: experimental DSC trace of an undeformed sample pre-annealed for 5000 s at 564 K. Dotted line: experimental DSC trace of an as-quenched sample.

The structural state of the specimens after the deformation was quenched-in by air cooling during de-evacuation of the vacuum chamber. Samples with a typical mass of 12.5 mg (approximately 2.5 cm of the ribbon) were used for the DSC experiments and were cut from within the deformed zone of the ribbon, but outside the failure zone. The DSC experiments were performed on a Perkin–Elmer DSC-7, using a crystallized PdNiP sample of approximately the same mass as a reference. All scans were made at a heating rate of 40 K/min up to a final temperature of 713 K. A second scan of the then crystallized sample is subtracted from the first scan for baseline correction. Details of the measurement procedure are given in Ref. [9]. The estimated accuracy of the DSC measurements is about 0.3 J/mol K.

4. RESULTS

Figure 1 shows tensile test curves of a-PdNiP measured at 564 K at the indicated strain rates $\dot{\varepsilon}$. All samples have been pre-annealed at 564 K for 5000 s, which is long enough to bring the material into its metastable equilibrium state at this temperature [9]. All curves manifest the phenomenon of strain softening, after which the flow stress levels off to a plateau value after about 15% deformation. Both the magnitude of the strain softening effect and the plateau value of the flow stress increase with increasing strain rate. Figure 2 shows

the DSC traces for the samples from Fig. 1 after the deformation. DSC traces of an as-quenched sample and an undeformed sample that was given an identical annealing treatment as the samples of Fig. 1 are also given. The DSC trace for the as-quenched sample, which has a highly disordered structural state, shows a small glass transition peak, preceded by a broad, shallow exothermal peak. The pre-equilibrated sample, which has the most ordered structural state obtainable by thermal treatment at 564 K, shows a pronounced glass transition peak. The broad exothermal peak is absent. The pre-equilibrated and subsequently deformed samples show a clear decrease in the height of the glass transition peak with increasing strain rate. Figure 2 therefore directly shows the influence of the deformation on the structural state of the metallic glass, namely deformation causes a disordering of the structure, which becomes more pronounced with increasing deformation rate. A similar series of experiments was also performed at 549 and 556 K, showing qualitatively the same results. In all tensile tests the plateau in σ was reached.

In order to characterize the structural state after the deformation the free volume is used as a parameter to quantify the state of short range order. The free volume after the high temperature deformation can be obtained from the DSC measurements as explained in Section 2: experimental DSC traces are reproduced using equations (2)–(4), in which the parameter x_0, being the free volume at the start of each scan, is the only parameter that is varied to obtain a good reproduction. The material parameters B, T_0, v_r and Q_r used in the calculations are taken from Ref. [9]. Since for deformed samples x_0 equals the quenched-in free volume after deformation x_d, a quantitative relation between x_d and the deformation temperature and strain rate is obtained. The reproductions of the DSC traces of Fig. 2 are given in Fig. 3. Figure 4 gives x_d as a function of the strain rate $\dot{\varepsilon}$ at the three deformation temperatures 549, 556 and 564 K. The thermal equilibrium values x_{eq} for the three temperatures are indicated next to the vertical axis. The error bars in x_d are estimated from the error in the DSC measurement. For large values of the free volume x_d the error is relatively large, because in this region the glass transition peak becomes rather insensitive to the actual value of x_d. The flow defect concentration after deformation $c_f^* = \exp(-1/x_d)$, normalized to the thermal equilibrium defect concentration $c_{f,eq}$, is given in Fig. 5 as a function of the strain rate for the three deformation tempera-

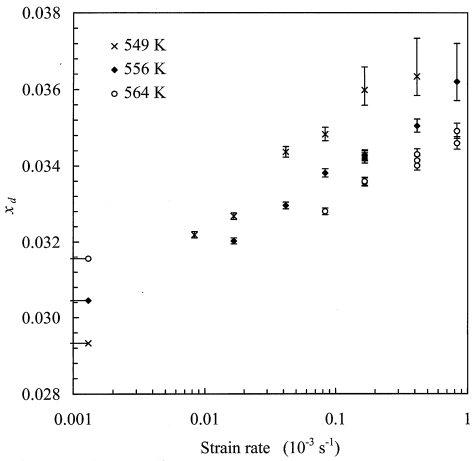

Fig. 4. The free volume after deformation x_d as a function of the strain rate at the indicated temperatures. The symbols near the x_d-axis give the thermal equilibrium values.

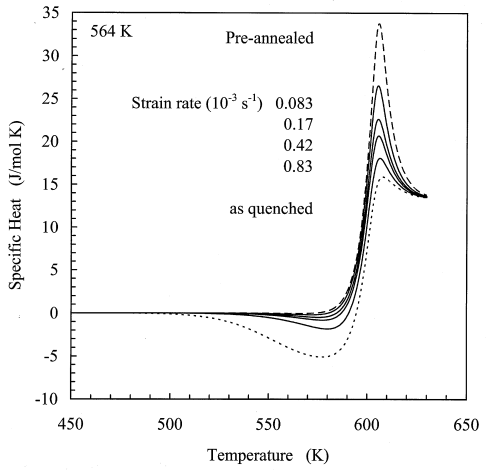

Fig. 3. Solid lines: calculated DSC traces of the samples from Fig. 1 after the deformation. Dashed line: calculated DSC trace of an undeformed sample pre-annealed for 5000 s at 564 K. Dotted line: calculated DSC trace of an as-quenched sample. The curves are to be compared with those of Fig. 2.

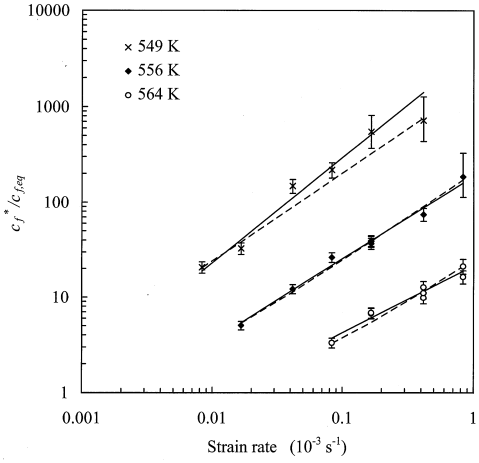

Fig. 5. The flow defect concentration after deformation c_f^* as a function of the strain rate at the indicated temperatures. Solid lines: least squares fits to $c_f^* \propto \dot{\varepsilon}^n$. Dashed lines: least squares fits to equation (9).

Table 1. Summary of experimental values obtained for $n = \partial \ln c_f^*/\partial \ln \dot{\varepsilon}$, $(\partial \sigma^*/\partial \ln \dot{\varepsilon})_{c_f=c_f^*}$, the strain rate sensitivity $m = \partial \ln \sigma_f^*/\partial \ln \dot{\varepsilon}$ and the proportionality factor a_x for production of free volume for the three deformation temperatures

T (K)	n	$(\partial \sigma^*/\partial \ln \dot{\varepsilon})_{c_f=c_f^*}$ (MPa)	m	a_x
549	1.10 ± 0.11	70 ± 7	0.18 ± 0.02	0.069 ± 0.007
556	0.87 ± 0.07	66 ± 7	0.23 ± 0.02	0.043 ± 0.004
564	0.70 ± 0.10	74 ± 12	0.26 ± 0.04	0.023 ± 0.002

tures, 549, 556 and 564 K. It is seen from Fig. 5 that the relation between c_f^* and $\dot{\varepsilon}$ can, at least for $c_f^* \gg c_{f,eq}$, be described reasonably well with the power law behaviour $c_f^* \propto \dot{\varepsilon}^n$, as given by the solid lines. The exponent $n = \partial \ln c_f^*/\partial \ln \dot{\varepsilon}$ for the three measuring temperatures are 1.10 ± 0.11, 0.87 ± 0.07 and 0.70 ± 0.10, respectively (Table 1).

In Fig. 6 the plateau value of the flow stress, denoted by σ^*, as a function of the strain rate is given for the three deformation temperatures. The logarithmic increments $(\partial \sigma^*/\partial \ln \dot{\varepsilon})_{c_f=c_f^*}$ are given in Table 1 and appear to be independent of the temperature within the experimental accuracy. The strain rate sensitivity $m = \partial \ln \sigma^*/\partial \ln \dot{\varepsilon}$ for the three temperatures is also given in Table 1.

It must be emphasized here that the values of x_d in Fig. 4 and c_f^* in Fig. 5 apply to the structural state that was frozen in after the deformation, i.e. they correspond to the structural state of the material at the plateau in the tensile tests. In order to investigate the relation between the flow stress and the structural state *during* the softening, a series of stress–strain curves was measured at 556 K and $\dot{\varepsilon} = 1.7 \times 10^{-4}$/s on samples that were pre-equilibrated by annealing for 10^4 s at 556 K. Each test was interrupted at a certain stage during the deformation, after which the free volume of the sample was determined from a DSC measurement. In Fig. 7 the stress–strain curves and the free volume x as a function of the strain are given. Figure 7 shows that the softening phenomenon is directly related to the disordering of the material; the decrease in the flow stress during the tensile test is related to an increase in the free volume. Plotting the flow stress σ at the interruption as a function of the flow defect concentration [derived from the free volume by equation (3)] yields a logarithmic increment $(\partial \sigma/\partial \ln c_f)_{\dot{\varepsilon},T} = -(120 \pm 40)$ MPa (Fig. 8). The first data point, which corresponds to the maximum stress in the tensile test curves of Fig. 7, was omitted from the fit, because at this stage the anelastic contribution to the strain is expected to have an appreciable magnitude, and the flow is therefore not purely plastic.

In order to investigate the effect of the pre-annealing treatment, in Fig. 9 tensile test curves, measured at 556 K and $\dot{\varepsilon} = 1.7 \times 10^{-4}$/s, are given for samples pre-annealed at 556 K for 120, 720 and 10^4 s, where the longest pre-annealing time is sufficient to bring the material in thermal equilibrium.

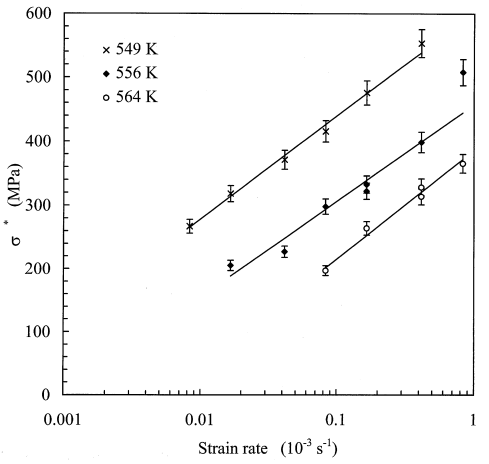

Fig. 6. The plateau value of the flow stress, σ^*, as a function of the strain rate at the indicated temperatures. Solid lines: least squares fits with a constant logarithmic increment $(\partial \sigma^*/\partial \ln \dot{\varepsilon})_{c_f=c_f^*}$ at each temperature.

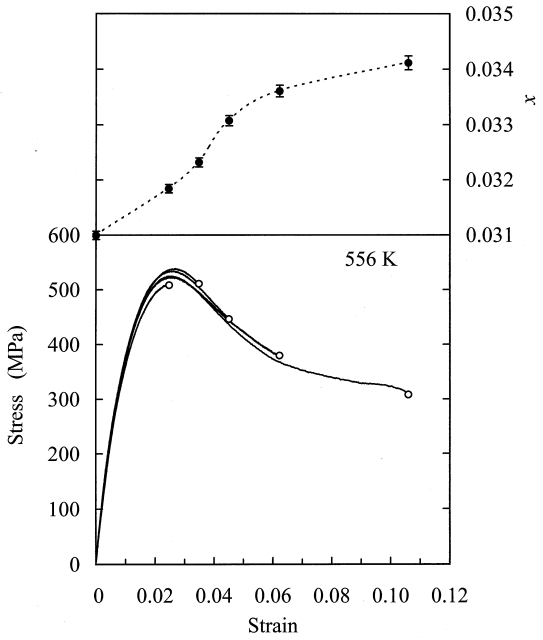

Fig. 7. Lower part: true stress vs true strain curves for five samples of a-PdNiP, pre-annealed for 10^4 s at 556 K, measured at 556 K and $\dot{\varepsilon} = 1.7 \times 10^{-4}$/s interrupted at the strains indicated by the open circles. Upper part: free volume after deformation as a function of the strain, as measured for the samples of the lower part of the figure. The dashed line is a guide to the eye.

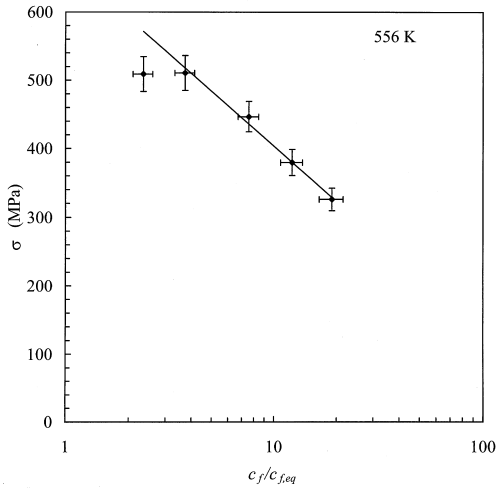

Fig. 8. The flow stress σ at the interruptions (Fig. 7) as a function of the defect concentration. The symbols are the data of Fig. 7. Solid line: least squares fit with a constant logarithmic increment $(\partial\sigma/\partial \ln c_f)_{\dot{\varepsilon},T}$.

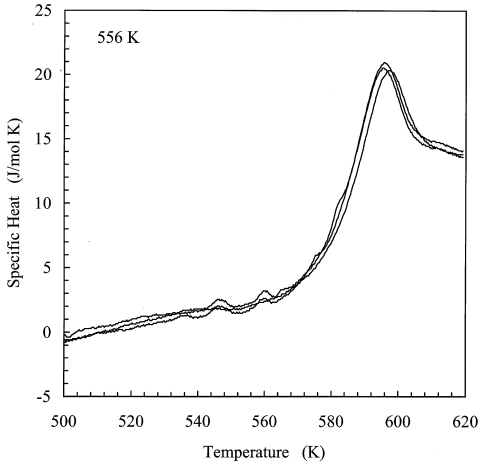

Fig. 10. DSC traces of the samples from Fig. 9 after the deformation.

In the pre-equilibrated sample a large strain softening effect is observed, similar to the previously presented results. The strain softening effect is less pronounced in the sample that was pre-annealed for 720 s, and in the sample with the shortest pre-annealing time strain softening is completely absent. Instead, strain hardening behaviour is found. Figure 9 shows that the plateau value of the flow stress is independent of the pre-annealing time; the small variations can be completely accounted for by the uncertainty in the cross-sectional area of the samples. The DSC traces of the samples after the deformation, shown in Fig. 10, are identical, i.e. the structural state of the samples after the high temperature deformation is independent of the structural state prior to the deformation. The difference in the tensile behaviour of the three samples therefore must be due to a different approach towards the final structural state, which depends on the pre-annealing time.

In order to test the reversibility of the structural changes, a strain rate cycling experiment was performed. Figure 11 shows a stress–strain curve measured at 556 K with an initial strain rate $\dot{\varepsilon} = 8.3 \times 10^{-5}$/s on a sample pre-annealed for 3600 s at 556 K. At $\varepsilon = 0.125$ the strain rate was increased instantaneously to 4.2×10^{-4}/s, resulting in a rapid increase of the stress, followed by a large strain softening effect. At $\varepsilon = 0.272$ the strain rate was decreased back to 8.3×10^{-5}/s. Now, after an initial rapid decrease in the stress, strain hardening is observed until the flow stress finally levels off at the

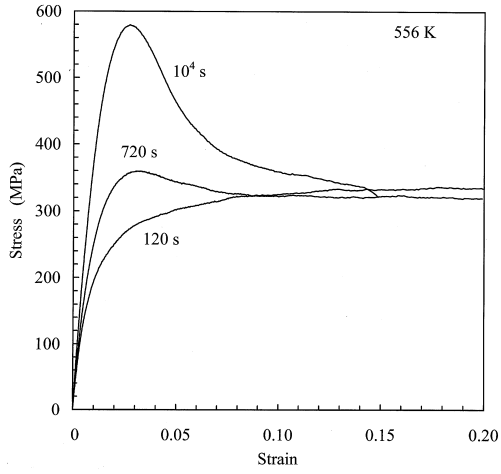

Fig. 9. True stress vs true strain curves for a-PdNiP, pre-annealed at 556 K for the indicated times, measured at 556 K and $\dot{\varepsilon} = 1.7 \times 10^{-4}$/s.

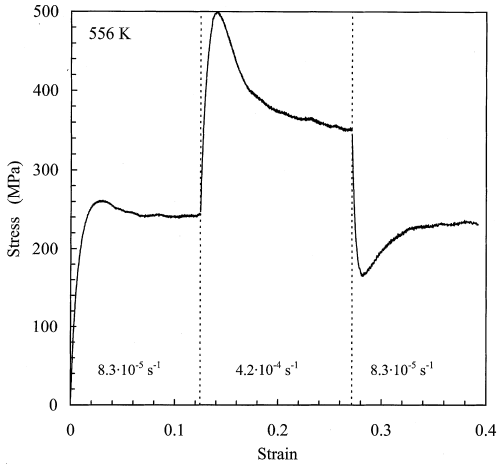

Fig. 11. True stress vs true strain curve for a-PdNiP, pre-annealed for 3600 s at 556 K and measured at 556 K. The strain rate was cycled between $\dot{\varepsilon} = 8.3 \times 10^{-5}$ and 4.2×10^{-5}/s.

same plateau value as in the first stage of the experiment. The transient effects indicate that reversible structural changes occur after the changes in the strain rate.

5. DISCUSSION

5.1. Deformation induced disordering

The measurements presented in the previous section unambiguously show that plastic deformation of a-PdNiP enhances the disorder in the structure of the material. As evidenced by the DSC measurements of Fig. 2, the free volume after deformation is larger than the thermal equilibrium value and increases with increasing strain rate. The evolution of the free volume during the deformation of the pre-equilibrated samples (Fig. 7) shows the direct relation between the strain softening and the increasing free volume, which can be understood from equation (1): with increasing defect concentration, the stress necessary to comply with the imposed strain rate decreases. The fact that the flow stress reaches a plateau value after a certain amount of deformation therefore indicates that the free volume reaches a plateau value, which depends on the strain rate and on the temperature (Figs 4 and 5). The plateau values are independent of the state of the material prior to the deformation (Figs 9 and 10) and are reversible upon changing the strain rate (Fig. 11). Thus, the plateau value can be recognized as an equilibrium value, which must be due to competition between deformation induced production of defects and thermal annihilation. Since all samples reached the plateau in σ, Figs 4 and 5 give the equilibrium values of the free volume after deformation x_d and the defect concentration c_f^*, respectively.

The approach towards equilibrium, depending on the history of the specimen, can give rise to either strain softening or strain hardening behaviour. In Fig. 9 it is seen that, depending on the pre-annealing time, either strain softening or strain hardening behaviour can occur, even at a single testing temperature and strain rate. For the sample pre-annealed for 120 s at 556 K the initial amount of free volume can be calculated, using the known kinetics of thermal structural relaxation [4], to be 0.0346. The free volume after deformation follows from a simulation of Fig. 10 and equals $x_d = 0.0342$ (see also Fig. 4). Because for this pre-annealing time the initial amount of free volume is larger than x_d, effectively only annihilation takes place during the test. Consequently, a monotonous increase of the flow stress is found until equilibrium is reached. For the samples pre-annealed for 720 and 10^4 s the initial free volume equals 0.0326 and 0.0307, respectively, i.e. lower than x_d. This is consistent with the observation that these samples show strain softening, and that the magnitude of the softening is larger for the longer pre-annealing time. This picture is confirmed by the strain rate cycling experiment of Fig. 11. In the first branch the free volume reaches its equilibrium value at $\dot{\varepsilon} = 8.3 \times 10^{-5}$/s, being $x_d = 0.0338$ (see Fig. 4). Upon the instantaneous increase in the strain rate from 8.3×10^{-5} to 4.2×10^{-4}/s the stress increases in order to comply with the imposed strain rate. As time proceeds, the amount of free volume gradually increases to $x_d = 0.0350$, the equilibrium at $\dot{\varepsilon} = 4.2 \times 10^{-4}$/s. This causes the strain softening effect in the second branch. In the third branch in Fig. 11 the opposite effect takes place.

It is clear from the above that equation (2), giving only the thermal annihilation and production kinetics of the defect concentration, must be modified in order to describe the evolution of the defect concentration during deformation. A straightforward way of doing this is adding a production term $P(c_f,\dot{\varepsilon},T)$ to the equation to account for the deformation induced disordering:

$$\frac{dc_f}{dt} = -k_r c_f (c_f - c_{f,eq}) + P(c_f,\dot{\varepsilon},T). \tag{7}$$

In order to investigate the deformation induced disordering we will consider here two phenomenological models. The first model assumes that during a flow event a number of defects are created, in a way similar to the creation of dislocations in crystalline materials. This implies that $dc_f \propto d\varepsilon$, in which case $P(c_f,\dot{\varepsilon},T) = a_f\dot{\varepsilon}$, with a_f a proportionality factor which may depend on temperature. Substituting this expression into equation (7), the strain rate dependent equilibrium defect concentration is found by the requirement that in equilibrium $dc_f/dt = 0$ for $c_f = c_f^*$, or

$$c_f^* = \frac{1}{2}\left(c_{f,eq} + \sqrt{c_{f,eq}^2 + 4a_f\dot{\varepsilon}/k_r}\right). \tag{8}$$

Note that $c_{f,eq}$ is the thermal equilibrium defect concentration, or $c_f^*(\dot{\varepsilon} = 0) = c_{f,eq}$. This model predicts that the logarithmic increment $n = \partial \ln c_f^* / \partial \ln \dot{\varepsilon}$ has an upper limit of 0.5 for large $\dot{\varepsilon}$ or $c_f^* \gg c_{f,eq}$. This upper limit for n is considerably lower than the experimentally observed values. Consequently, no satisfactory fit of equation (8) to the data of Fig. 5 can be obtained.

The second model assumes that during a flow event a certain amount of free volume dx is introduced, which redistributes over the atoms and thus increases the defect concentration. Using equation (3) it follows that $P(c_f,\dot{\varepsilon},T) = a_x\dot{\varepsilon}c_f \ln^2 c_f$, with a_x a proportionality factor which may depend on temperature. Inserting this expression in equation (7) leads, with $dc_f/dt = 0$ for $c_f = c_f^*$, to

$$c_f^* = c_{f,eq} + (a_x/k_r)\dot{\varepsilon} \ln^2 c_f^*. \tag{9}$$

The model equation (9) predicts an upper limit for $n = \partial \ln c_f^* / \partial \ln \dot{\varepsilon}$ close to unity for large $\dot{\varepsilon}$. The

dashed lines in Fig. 5 are least squares fits to equation (9), with a_x as a free parameter and $c_{f,eq}$ and k_r calculated from the material parameters obtained in Ref. [9]. As can be seen, equation (9) describes the relation between c_f^* and $\dot{\varepsilon}$ quite well. The values of a_x, given in Table 1, show a significant decrease with increasing temperature.

The model expression $P(c_f,\dot{\varepsilon},T) = a_x\dot{\varepsilon}c_f \ln^2 c_f$ is based solely on the equilibrium values for the defect concentration as a function of the strain rate. Another test of the model is to consider the kinetics of the deformation induced disordering, using the experimental evidence provided by Figs 1 and 7. Figure 1 shows that the equilibrium is reached at $\varepsilon \approx 0.15$ for all strain rates, although the equilibration becomes slightly slower with increasing strain rate. In the lower part of Fig. 12 the numerical solution to equation (7) is given for the four strain rates at $T = 564$ K. The upper part of Fig. 12 shows the experimental data of Fig. 7 and the calculated free volume x as a function of the strain at $T = 556$ K and $\dot{\varepsilon} = 1.7 \times 10^{-4}$/s. The calculations were carried out using the simplification that the plastic flow rate equals the imposed strain rate at all times, which under the experimental conditions is not the case for strains up to $\varepsilon \approx 0.02$. This means that for $\varepsilon \leq 0.02$ the calculated kinetics is somewhat too fast. The calculated curves in Fig. 12 show the correct tendencies, namely equilibration at $\varepsilon \approx 0.15$, with some retardation at higher strain rates, but the overall conclusion seems that the calculated kinetics, also regarding the data from Fig. 7, is slightly too slow.

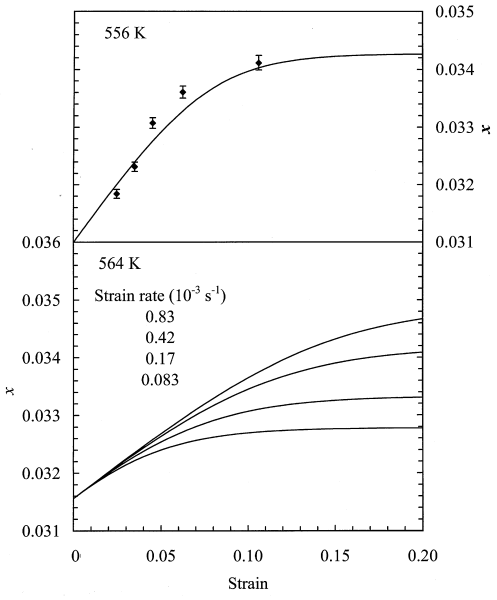

Fig. 12. Lower part: free volume as a function of the strain, calculated using equation (7), at 564 K and the indicated strain rates. Upper part: free volume as a function of the strain at 564 K and $\dot{\varepsilon} = 1.7 \times 10^{-4}$/s. The symbols are the experimental data of Fig. 7, the solid line is calculated using equation (7).

We conclude that the assumption $dx \propto d\varepsilon$ reproduces the basic features of the deformation induced disordering rather well. The quantitative agreement with the experimental data is reasonable, considering that both the equilibrium defect concentration and the kinetics of the deformation induced disordering can be described with a single adjustable parameter a_x. The physical interpretation of the assumption $dx \propto d\varepsilon$ is that the local ordering of the atoms participating in the flow event is perturbed due to the event, resulting in an increase in the free volume, which subsequently gradually redistributes over the structure. The temperature dependence of the proportionality factor a_x that we have found, i.e. decreasing with increasing temperature, can be explained by a partial restoring of the local order during the flow event due the thermal motion of the atoms.

The amount of free volume created in a single flow event can be derived as follows. Following Spaepen's model for plastic flow, a single flow event with a local strain ε_0 produces a macroscopic strain $\Delta\varepsilon$ given by

$$\Delta\varepsilon = \frac{\varepsilon_0 v_0}{V}\tanh\left(\frac{\sigma\varepsilon_0 v_0}{2kT}\right) \tag{10}$$

with V the volume of the specimen. The factor $\tanh(\sigma\varepsilon_0 v_0/2kT)$ is the fraction of the flow events in the direction of the external stress, which, for sufficiently large stresses, equals 1. As will be derived later, $\varepsilon_0 v_0 = 130$ A^3 for a-PdNiP at 556 K, which makes the assumption $\tanh(\sigma\varepsilon_0 v_0/2kT) \approx 1$ valid for all flow stresses in our experiments. The deformation $\Delta\varepsilon$ induces an amount of reduced free volume $\Delta x = a_x\Delta\varepsilon$. Using the definition $x = \langle v\rangle/\gamma v^*$ and $\langle v\rangle = V_f/N$, with V_f the total amount of free volume and N the total number of atoms, and $V = N\Omega$, with Ω the mean atomic volume, the total amount of free volume ΔV_f created per flow event is found to be

$$\Delta V_f = a_x\frac{\varepsilon_0 v_0}{\Omega}\gamma v^*. \tag{11}$$

Inserting $a_x = 0.043$ at $T = 556$ K, $\varepsilon_0 v_0 = 130$ A^3 and $\gamma v^* \approx 0.5\Omega$ we find $\Delta V_f = 3$ A^3 or approximately 0.2Ω, which seems a physically plausible value. It seems unlikely that the rather strong temperature dependence of a_x, which we have found, can be extrapolated to lower temperatures, as this would lead to unphysical high values for ΔV_f. Irrespective of the exact temperature dependence of a_x, the production term $P(c_f,\dot{\varepsilon},T) = a_x\dot{\varepsilon}c_f \ln^2 c_f$ in equation (7) becomes a dominant factor in the kinetics of structural relaxation at temperatures far below T_g, since the rate factor for annihilation k_r decreases rapidly with decreasing temperature. The production of free volume during plastic deformation therefore also accounts for the occurrence

of localized shear at low temperatures, visible as thin shear bands on the surface of the deformed glass [18]. Spaepen and Turnbull [19] were the first to propose that this inhomogeneous deformation is due to a catastrophic production of free volume. Later, this concept has been elaborated by Spaepen [20] and Steif *et al.* [21] on the basis of assumed relations for the production of free volume during plastic deformation. The present work corroborates this supposition. If, due to a fluctuation or at some stress concentrator, in a certain region of the sample a temporary increase in strain rate occurs, this leads locally to an increased defect concentration. The increased defect concentration in turn leads to an even higher local strain rate, if it is not counteracted by thermal annihilation of defects. This latter condition is satisfied at low temperatures (low k_r) and at high strain rates. Eventually this can lead to layers in the material that can be considered fluid, appearing as shear bands and a vein-like fracture surface [18].

5.2. Plastic flow

In the initial stages of a tensile test the strain is mostly elastic and anelastic. With increasing stress the plastic flow rate contribution to the total strain rate increases and rapidly becomes the dominant contribution. At this stage the flow stress σ is, according to equation (1), given by

$$\sigma = \frac{2kT}{\varepsilon_0 v_0} \operatorname{arcsinh}\left(\frac{\dot{\varepsilon}\Omega}{2c_f k_f \varepsilon_0 v_0}\right) \tag{12}$$

which can be approximated, with a high degree of accuracy, to

$$\sigma = \frac{2kT}{\varepsilon_0 v_0} \ln\left(\frac{\dot{\varepsilon}\Omega}{c_f k_f \varepsilon_0 v_0}\right) \tag{13}$$

for $\sigma\varepsilon_0 v_0/2kT$ larger than about 2, an assumption that appears to be valid considering the data in Fig. 8 and that will be verified later.

Using equation (13) the following quantities can be derived:

1. At constant strain rate and temperature equation (13) yields $(\partial\sigma/\partial \ln c_f)_{\dot{\varepsilon},T} = -2kT/\varepsilon_0 v_0$. From the experimental value of $-(120 \pm 40)$ MPa derived from Fig. 8 it follows that $\varepsilon_0 v_0 = 130 \pm 50$ Å^3 at $T = 556$ K and $\sigma\varepsilon_0 v_0/2kT > 2$ for $\sigma > 230$ MPa, which validates the use of equation (13) instead of equation (12).
2. At constant defect concentration and temperature equation (13) yields $(\partial\sigma/\partial \ln \dot{\varepsilon})_{c_f,T} = 2kT/\varepsilon_0 v_0$. A test of this quantity would require the measurement of σ at different strain rates and constant c_f. This is hampered by elastic and anelastic effects and by structural relaxation occurring after a change in $\dot{\varepsilon}$, as is visible in Fig. 11. Figure 7 shows that at the maximum stress in the tensile curve some additional free volume has already been created. Therefore, only the lower limit for $(\partial\sigma/\partial \ln \dot{\varepsilon})_{c_f,T}$ can be estimated from Fig. 11. From the plateau value of the flow stress at $\dot{\varepsilon} = 8.3 \times 10^{-5}$/s and the maximum stress at $\dot{\varepsilon} = 4.2 \times 10^{-4}$/s it is found that $(\partial\sigma/\partial \ln \dot{\varepsilon})_{c_f,T} > 160$ MPa. This yields $\varepsilon_0 v_0 < 96$ Å^3, a value which is not inconsistent with the previously obtained result within the experimental accuracy, but appears to be rather low considering that it is an upper bound.
3. For the plateau value of the flow stress, where $c_f = c_f^*$, it follows from equation (13) that $(\partial\sigma^*/\partial \ln \dot{\varepsilon})_{c_f=c_f^*} = (2kT/\varepsilon_0 v_0)(1 - \partial \ln c_f^*/\partial \ln \dot{\varepsilon})$. Experimentally, this quantity was found to be 70 MPa (see Table 1), independent of temperature. Using the experimental values for $\partial \ln c_f^*/\partial \ln \dot{\varepsilon}$ from Table 1 results in partly unphysical values for $\varepsilon_0 v_0$. Using the model expression (9) (the dashed lines in Fig. 5) results in values for $\varepsilon_0 v_0$ that range from 16 to 40 Å^3 for the three deformation temperatures, which is inconsistent with the previous results.

From the above it is clear that equation (1) does not adequately describe all the aspects of plastic flow. Our results suggest that a relation of the form

$$\sigma = \sigma_0(\dot{\varepsilon}) + \frac{2kT}{\varepsilon_0 v_0} \ln\left(\frac{\dot{\varepsilon}\Omega}{c_f k_f \varepsilon_0 v_0}\right) \tag{14}$$

is more realistic. The quantity $\sigma_0(\dot{\varepsilon})$ can be identified as a threshold stress which should depend on the strain rate but not on the defect concentration. Using equation (14) for the three quantities discussed before, leads to the following observations:

1. $(\partial\sigma/\partial \ln c_f)_{\dot{\varepsilon},T} = -2kT/\varepsilon_0 v_0 = -(120 \pm 40)$MPa and therefore $\varepsilon_0 v_0 = 130 \pm 50$ Å^3 is not affected.
2. $(\partial\sigma/\partial \ln \dot{\varepsilon})_{c_f,T} = (\partial\sigma_0/\partial \ln \dot{\varepsilon}) + 2kT/\varepsilon_0 v_0 > 160$ MPa. This experimental quantity leads, with $\varepsilon_0 v_0 = 130 \pm 50$ Å^3, to the result $(\partial\sigma_0/\partial \ln \dot{\varepsilon}) > 54$ MPa.
3. $(\partial\sigma^*/\partial \ln \dot{\varepsilon})_{c_f=c_f^*} = (\partial\sigma_0/\partial \ln \dot{\varepsilon}) + (2kT/\varepsilon_0 v_0)(1 - \partial \ln c_f^*/\partial \ln \dot{\varepsilon})$. It then follows, using $\varepsilon_0 v_0 = 130 \pm 50$ Å^3 and the values given in Table 1, that $\partial\sigma_0/\partial \ln \dot{\varepsilon} \approx 60$, 50 and 50 MPa at 549, 556 and 564 K, respectively. The result for $(\partial\sigma_0/\partial \ln \dot{\varepsilon})$ at $T = 556$ K is consistent with point (2) within the estimated uncertainties.

The existence of a threshold stress has previously been suggested by Taub [22], who attributed the threshold stress to an increase of the internal energy of the material, which could be used, for instance, to reduce the local ordering. However, in Taub's work, the threshold stress was found to be independent of the strain rate and considerably smaller than the flow stresses in our experiments. At this point, we can not give an adequate explanation for the strain rate dependence of σ_0 and the basic assumption, i.e. σ_0 is independent of c_f, remains to be verified. New experiments are currently being performed in order to clarify this point.

6. CONCLUSIONS

We have shown, using a combination of tensile test and DSC measurements, that homogeneous plastic deformation of amorphous $Pd_{40}Ni_{40}P_{20}$ at temperatures close to the glass transition temperature disorders the structure of the material. Within Spaepen's model of plastic flow, the disordering can be explained by the assumption that the local order is perturbed during a flow event, resulting in an increase in the free volume. The rate of production of free volume is proportional to the strain rate. Due to the competition with thermal annihilation of defects, the material eventually reaches a strain rate dependent equilibrium state. A detailed analysis of the stress–strain curves indicates the existence of a strain rate dependent threshold stress for plastic flow.

REFERENCES

1. Taub, A. I. and Spaepen, F., *Acta metall.*, 1980, **281**, 781.
2. Tsao, S. S. and Spaepen, F., *Acta metall.*, 1985, **33**, 881.
3. van den Beukel, A., Huizer, E., Mulder, A. L. and van der Zwaag, S., *Acta metall.*, 1986, **34**, 483.
4. Duine, P. A., Sietsma, J. and van den Beukel, A., *Acta metall. mater.*, 1992, **40**, 743.
5. Inoue, A., Nakamura, T., Nishiyama, N., Sugita, T. and Masumoto, T., *Key Engng Mater.*, 1993, **81-83**, 147.
6. Mulder, A. L., Van der Zwaag, S. and van den Beukel, A., *Scripta metall.*, 1983, **17**, 1399.
7. Wu, T. W. and Spaepen, F., *Acta metall.*, 1985, **33**, 2185.
8. Inoue, A., Zhang, T. and Masumoto, T., *J. Non-Cryst. Solids*, 1990, **156-158**, 598.
9. Tuinstra, P., Duine, P. A., Sietsma, J. and van den Beukel, A., *Acta metall. mater.*, 1995, **43**, 2815.
10. Spaepen, F., in *Physics of Defects*, Les Houches Lectures XXXV, ed. R. Balian *et al.*, 1980, p. 135.
11. Taub, A. I., *Acta metall.*, 1980, **28**, 633.
12. Cohen, M. H. and Turnbull, D., *J. Chem. Phys.*, 1959, **31**, 1164.
13. Koebrugge, G. W., Sietsma, J. and van den Beukel, A., *Acta metall. mater.*, 1992, **40**, 753.
14. de Hey, P., Sietsma, J. and van den Beukel, A., *Nanostructured and Non-crystalline Materials, Proc. IV Int. Workshop on Non-Cryst. Solids*, ed. M. Vásquez and A. Hernando. World Scientific, Singapore, 1995, p. 347.
15. van den Beukel, A. and Sietsma, J., *Acta metall. mater.*, 1990, **38**, 383.
16. Davis, L. A., Chou, C.-P., Tanner, L. E. and Ray, R., *Scripta metall.*, 1976, **10**, 937.
17. de Hey, P., Sietsma, J. and van den Beukel, A., *J. Non-Cryst. Solids*, 1996, **205-207**, 696.
18. Spaepen, F., *Acta metall.*, 1975, **23**, 615.
19. Spaepen, F. and Turnbull, D., *Scripta metall.*, 1974, **8**, 563.
20. Spaepen, F., *Acta metall.*, 1977, **25**, 407.
21. Steif, P. S., Spaepen, F. and Hutchinson, J. W., *Acta metall.*, 1982, **30**, 447.
22. Taub, A. I., *Acta metall.*, 1982, **30**, 2117.